

www.acsabm.org Article

Enhanced Bacterial Growth by Polyelemental Glycerolate Particles

Abhijit H. Phakatkar, Josué M. Gonçalves, Jianshu Zhou, Timothy G. Ritter, Mahmoud Tamadoni Saray, Lioudmila V. Sorokina, Azadeh Amiri, Lucio Angnes, Tolou Shokuhfar,* and Reza Shahbazian-Yassar*



Cite This: ACS Appl. Bio Mater. 2023, 6, 1515–1524



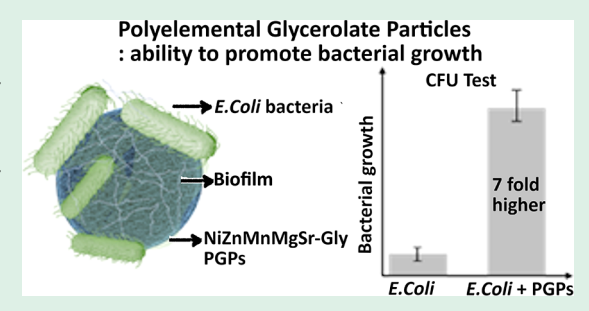
ACCESS I

III Metrics & More

Article Recommendations

Supporting Information

ABSTRACT: While polyelemental alloys are shown to be promising for healthcare applications, their effectiveness in promoting bacterial growth remains unexplored. In the present work, we evaluated the interaction of polyelemental glycerolate particles (PGPs) with Escherichia coli (E. coli) bacteria. PGPs were synthesized using the solvothermal route, and nanoscale random distribution of metal cations in the glycerol matrix of PGPs was confirmed. We observed 7-fold growth of E. coli bacteria upon 4 h of interaction with quinary glycerolate (NiZnMnMgSr-Gly) particles in comparison to control E. coli bacteria. Nanoscale microscopic studies on bacteria interactions with PGPs showed the release of metal cations in the bacterium cytoplasm from PGPs. The electron microscopy imaging and



chemical mapping indicated bacterial biofilm formation on PGPs without causing significant cell membrane damage. The data showed that the presence of glycerol in PGPs is effective in controlling the release of metal cations, thus preventing bacterial toxicity. The presence of multiple metal cations is expected to provide synergistic effects of nutrients needed for bacterial growth. The present work provides key microscopic insights of mechanisms by which PGPs enhance biofilm growth. This study opens the door for future applications of PGPs in areas where bacterial growth is essential including healthcare, clean energy, and the food industry.

KEYWORDS: polyelemental particles, bacterial growth, nano-/biointeractions, glycerolate materials, in situ graphene liquid cell, transmission electron microscopy

■ INTRODUCTION

Polyelemental materials¹⁻³ are an emerging class of materials with vast compositional space that can be tuned to promote the synergistic properties of alloyed materials for various applications ranging from clean energy^{4,5} to healthcare^{6,7} and structural materials. 1,8 Recent studies show the potential of polyelemental materials for biological applications such as antibacterial agents ^{9–11} or medical implants. ^{12,13} Polyelemental alloys possess excellent mechanical and chemical stability attributing to their configurational mixing entropy. 14 Alamdari et al. reported the substantial 98.5% antibacterial efficacy of the TiZrTaNbWAg polyelemental film against Escherichia coli (E. coli) bacteria. Murray et al. 10 reported the 6.4 log reduction of the double-stranded deoxyribonucleic acid (DNA) activity of E. coli bacteria after interacting with the CoCuAgNiSi polyelemental film. Chen et al. 15 evaluated 97.45% antibacterial efficacy of the CrFeNiCuSi polyelemental alloy against E. coli bacteria by exhibiting synergistic activity of multiple metal cations. However, it is yet to be reported the applications of such materials in promoting bacterial growth.

Expediting bacterial growth is of utmost importance for emerging microbial fuel cells, ice-binding proteins, and antifreeze proteins in research applications. In addition, probiotic bacteria possess a wide range of applications in the food industry and medicine avenues. Among various bacteria, *E. coli* bacteria lie at the center of the development of

biological systems considering their well-studied complex cellular structure and metabolism. In proteomic studies, *E. coli* bacteria can express heterologous recombinant proteins with superior tunability.²³ As a result, new and affordable approaches are needed in improving *E. coli* energy production and metabolism for industrial applications. However, the carbon flux in central bacterial cellular metabolism can get deprived as a result of forced production of gene-encoding products, resulting in cell physiochemical energy depletion.^{24,25}

Glycerol is a cost-effective and abundantly available source of carbon for microorganisms for various metabolic activites. ²⁴ *E. coli* bacteria can metabolize glycerol to produce energy in the presence of external electron acceptors (respiratory metabolism) and also in the absence of electron acceptors by fermentative metabolism. ²⁶ In addition to glycerol, various metal ions in the lower concentrations are capable of improving bacterial cell metabolic activities. ²⁷ Metal ions act as essential cofactors for cellular protein functioning, structural

Received: December 20, 2022 Accepted: February 16, 2023 Published: March 18, 2023





Figure 1. Schematic representation of polyelemental glycerolate particles synthesis using the solvothermal method. Equimolar concentrations of the precursor metal salts of Mn, Mg, Zn, Ni, and Sr were homogeneously mixed in solvent. The prepared solution was heated at 180 °C for 10 h in an autoclave mold. The final product was rinsed and thoroughly dried prior to use in probiotic applications.

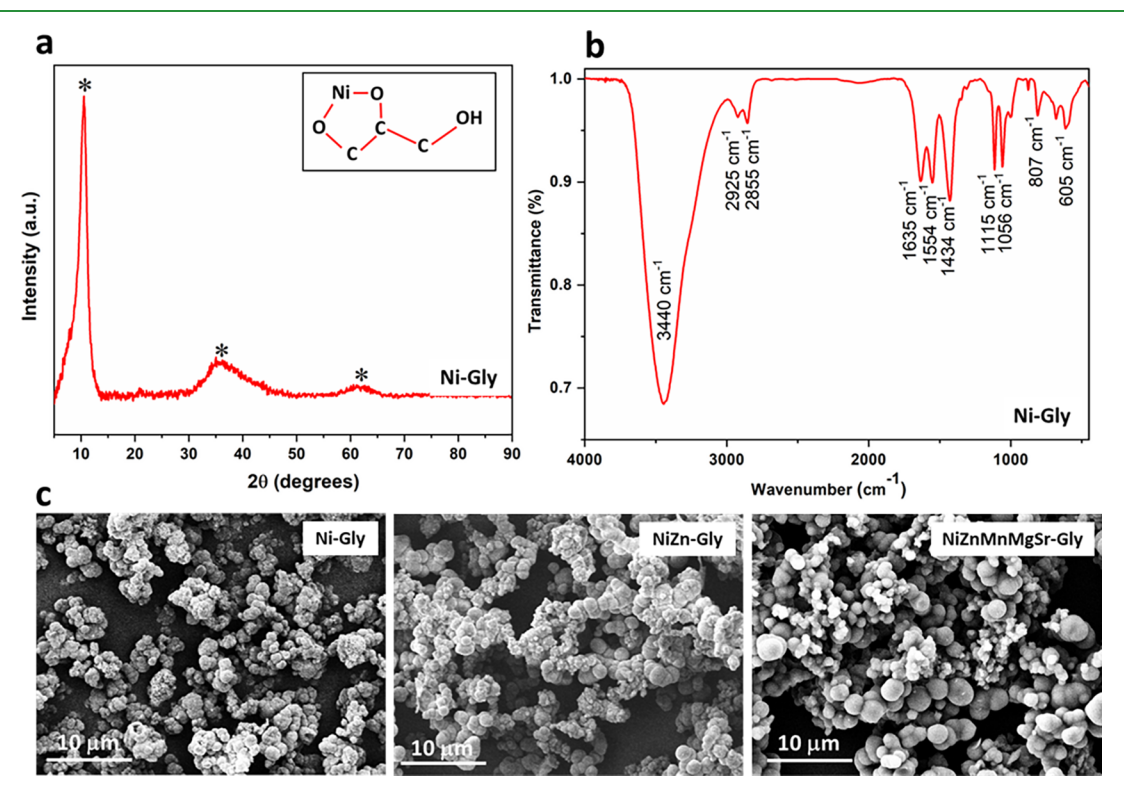


Figure 2. Structural and morphological evaluation of metal glycerolate particles. (a) XRD spectrum of unary Ni-Gly particles confirming their characteristic layered crystal structure. The inset shows the chemical coordination of Ni cations with the glycerol matrix. (b) FTIR spectrum of unary Ni-Gly particles revealing their molecular structure. (c) SEM micrographs of respective unary Ni-Gly, binary NiZn-Gly, and quinary NiZn-MnMgSr-Gly particles highlighting their spherical morphology.

stability, cell signaling, and virulence regulation.²⁸ Bacteria use metal ions for various cellular activities such as electron transfer, oxygen metabolism, signaling for biofilm formation, and functioning of DNA polymerases, adenosine triphosphatases (ATPases), and kinases.²⁹

In the present study, the microscopic interactions of *E. coli* bacteria with a novel category of polyelemental glycerolate particles (PGPs) are reported for the first time. The elemental

compositions of synthesized unary nickel glycerolate (Ni-Gly), binary nickel-zinc glycerolate (NiZn-Gly), and quinary nickel-zinc-manganese-magnesium-strontium glycerolate (NiZnMnMgSr-Gly) particles were evaluated using scanning transmission electron microscopy (STEM) and energy dispersive X-ray spectroscopy (EDS) techniques. Further bacterial growth upon interacting with PGPs was confirmed using an in vitro colony forming unit (CFU) test. The results

ACS Applied Bio Materials www.acsabm.org Article

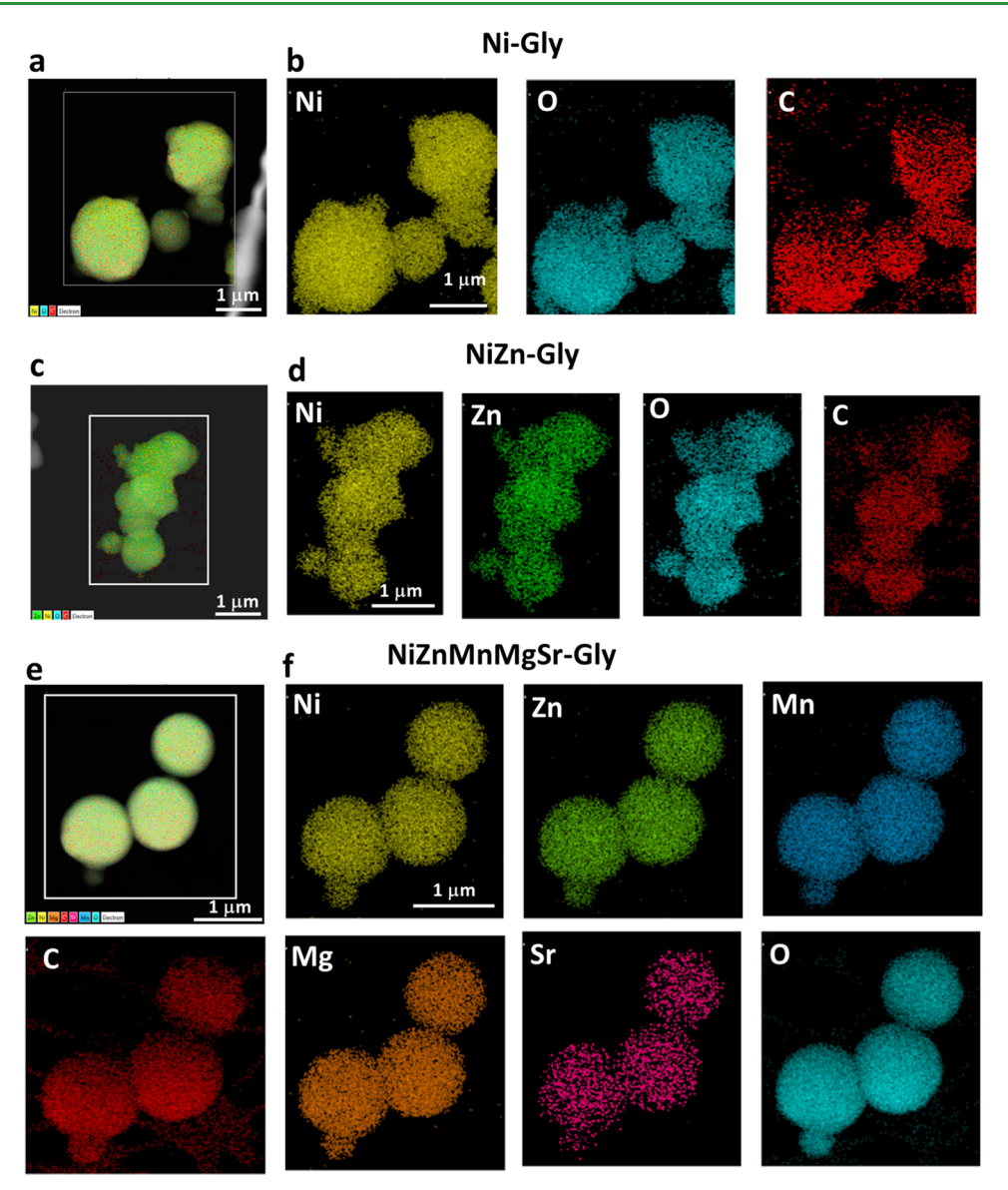


Figure 3. STEM-EDS elemental analysis of metal glycerolate particles. (a) Mixed elemental mapping of unary Ni-Gly particles confirming the presence of Ni, O, and C elements. (b) Corresponding elemental mapping of individual Ni, O, and C elements indicating the homogeneous distribution of Ni cations in the glycerol matrix. (c) Mixed elemental mapping of binary NiZn-Gly particles confirming the presence of Ni, Zn, O, and C elements. (d) Corresponding elemental mapping of individual Ni, Zn, O, and C elements indicating the homogeneous distribution of Ni and Zn elements in the glycerol matrix. (e) Mixed elemental mapping of quinary NiZnMNMgSr-Gly particles confirming the presence of Ni, Zn, Mn, Mg, Sr, O, and C elements. (f) Corresponding elemental mapping of individual Ni, Zn, Mn, Mg, Sr, O, and C elements confirming the uniform presence of metal cations in the glycerol matrix.

indicate a more than 7-fold increase in *E. coli* bacterial growth upon interacting with quinary-glycerolate particles as compared with control *E. coli* bacteria, while the enhanced growth of bacteria upon interacting with Ni-Gly and NiZn-Gly particles was 2.75- and 3.5-fold, respectively. To study the microscopic origins of the enhanced growth of *E. coli* bacteria, a solution mixture of bacteria and PGPs was investigated using graphene liquid cells (GLCs) in STEM.

RESULTS AND DISCUSSION

Figure 1 shows the synthesis process of PGPs, where the key process details are highlighted (see the Methods section for details). Briefly, the solvothermal method, as described by Mir et al., 30 was utilized to produce PGPs. Specifically, Ni-, 31 Zn-, 32 Mn-, 33 Mg-, 34 and Sr-35,36 based precursor salts were chosen as

metal coordination elements for PGPs due to the positive roles of such metals in enhancing bacterial growth. Table S1 summarizes the maximum tolerance limit of metal cations beneficial for bacteria metabolism. Briefly, the PGPs were synthesized by achieving coordination between multiple metal cations in the glycerol matrix using the solvothermal route. Metal glycerolate particles possess an interestingly layered structure of stacked metal-oxygen sheets bonded with glycerol anions. The coordination chemistry between multiple transition metal cations and glycerol molecules is further evaluated in the following sections.

Structural and morphological analyses of the as-synthesized PGPs were performed using X-ray diffraction (XRD), Fourier transform infrared (FTIR) spectroscopy, and scanning electron microscopy (SEM) characterization techniques. Figure 2

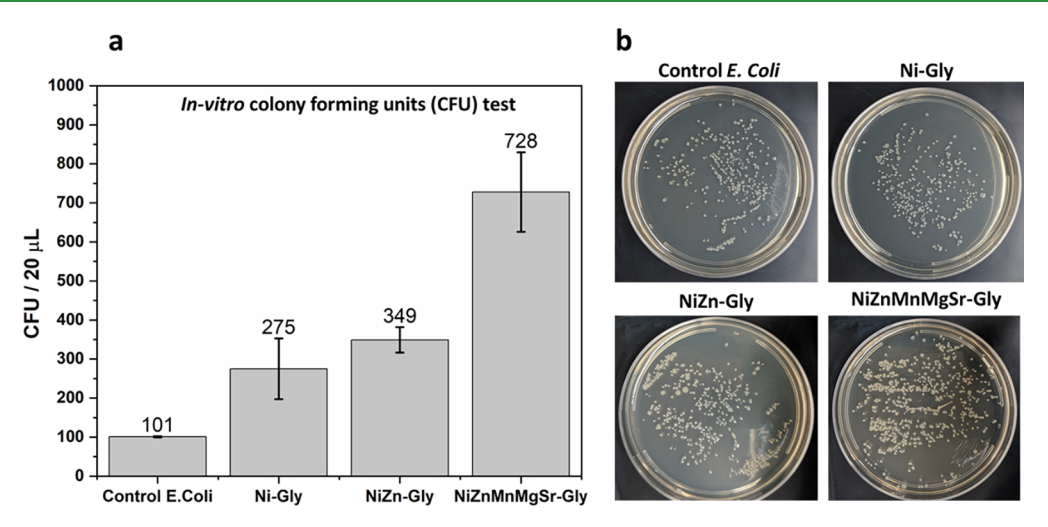


Figure 4. In vitro CFU test results of cultured *E. coli* bacterial interactions with polyelemental glycerolate particles. (a) CFU test results indicating the exponential growth of *E. coli* bacteria after 4 h of interaction with unary Ni-Gly, binary NiZn-Gly, and quinary NiZnMnMgSr-Gly particles at 100 µg/mL concentration. (b) Respective CFU test results highlighting the exponential growth of *E. coli* bacteria.

shows the XRD spectrum, FTIR spectrum, and SEM micrographs of as-synthesized unary Ni-Gly particles. As shown in the XRD spectrum in Figure 2a, an intense characteristic peak at $2\theta = 10.55^{\circ}$ was observed, which confirms the layered crystal structure of the as-synthesized Ni-Gly particles. 37,38 The characteristic broad peaks of the Ni-Gly particles at $2\theta = 35.85^{\circ}$ and $2\theta = 61.55^{\circ}$ confirmed the amorphous nature of the as-synthesized particles.^{37,39} Figure S1 shows similar XRD results for quinary NiZnMnMgSr-Gly particles. In these quinary glycerolate particles, a small fraction of the secondary phase of strontium carbonate (SrCO₃) is detected, but upon multiple STEM-EDS analyses, no significant phase segregation in NiZnMnMgSr-Gly particles was found, indicating that their presence is minimal. The formation of SrCO₃ is possibly due to the high activity of Sr ions with a small amount of CO2 in air dissolved in the solution and precipitation of SrCO₃. Similarly, Figure S2 shows the XRD spectrum for NiZn-Gly particles, where a small fraction of zinc carbonate hydroxide $((Zn)_5(CO_3)_2(OH)_6)$ secondary phase was detected.⁴¹ Figure 2b shows the FTIR spectrum of Ni-Gly particles, confirming the coordination between Ni cations in the glycerol matrix.⁴² In the FTIR spectrum, absorption bands at the 3440 cm⁻¹ wavenumber as well as wavenumbers at 2925 and 2855 cm⁻¹ are attributed to the characteristic hydrogen-bonded O-H group and C-H group stretching vibrations, respectively. The presence of absorbed water in the particles can be confirmed with respect to the bending vibrations of H-O-H bonds located at 1635 cm⁻¹. The bands near 1434 cm⁻¹ are attributed to O-H bending vibrations. Bands at the 1115 and 1056 cm⁻¹ wavenumbers are affiliated to C-H stretching vibrations. The lower end near the 605 cm⁻¹ bands correspond to metal oxygen stretching vibrations. In Figure 2c, the SEM micrographs of unary Ni-Gly, binary NiZn-Gly, and quinary NiZnMnMgSr-Gly particles are shown, which confirm the predominant presence of the spherical morphology of the assynthesized metal glycerolate particles.

Figure 3 shows the STEM-EDS elemental analysis of the PGPs. Figure 3a shows the STEM-EDS mixed elemental mapping of unary Ni-Gly particles, where the presence of Ni, O, and C elements was confirmed. Corresponding individual STEM-EDS elemental mapping of Ni, O, and C elements is

shown in Figure 3b, where the uniform distribution of Ni cations in the glycerol matrix can be confirmed. STEM-EDS elemental mapping of C and O elements is associated with the glycerol matrix in PGPs. Figure 3c shows the STEM-EDS mixed elemental mapping of binary NiZn-Gly particles, where the presence of Ni, Zn, O, and C elements was confirmed. Corresponding individual STEM-EDS elemental mapping images of Ni, Zn, O, and C elements are shown in Figure 3b, where the uniform distribution of Ni and Zn cations in the glycerol matrix was confirmed. The analyzed metal cation elemental composition in the glycerol matrix for NiZn-Gly particles was 57.60 ± 2.6 at % for Ni and 42.40 ± 2.6 at % for Zn. Figure 3e shows the STEM-EDS mixed elemental mapping of quinary NiZnMnMgSr-Gly particles, where the presence of Ni, Zn, Mn, Mg, Sr, O, and C elements was confirmed. The corresponding individual STEM-EDS elemental mapping images of Ni, Zn, Mn, Mg, Sr, O, and C elements are shown in Figure 3f, where the uniform distribution of Ni, Zn, Mn, Mg, and Sr cations in the glycerol matrix was determined. The analyzed metal cation elemental composition in the glycerol matrix for NiZnMnMgSr-Gly particles was 24.6 \pm 7.5 at % for Ni, 21.07 \pm 2.3 at % for Zn, 25.77 \pm 0.8 at % for Mn, 22.77 \pm 6.5 at % for Mg, and 5.8 \pm 1.3 at % for Sr. Respective STEMhigh angle annular dark field (HAADF) micrographs of unary Ni-Gly, binary NiZn-Gly, and quinary NiZnMnMgSr-Gly PGPs corresponding to STEM-EDS are shown in Figure S3.

The interaction between *E. coli* bacteria and PGPs was quantitatively evaluated using an *in vitro* colony counting method. ^{43,44} Figure 4 shows *in vitro* colony forming units (CFU) test results upon interacting cultured *E. coli* bacteria with unary Ni-Gly, binary NiZn-Gly, and quinary NiZnMnMgSr-Gly particles for 4 h at 100 μg/mL concentration. Figure 4a confirms the 2.75-fold, 3.5-fold, and 7.28-fold exponential growth of *E. coli* bacteria upon 4 h of interaction with unary Ni-Gly, binary NiZn-Gly, and quinary NiZnMnMgSr-Gly particles, respectively, in comparison with control *E. coli* bacteria that did not interact with PGPs. Respective bacterial concentrations of 101, 275, 349, and 728 CFU/20 μL of control *E. coli*, Ni-Gly, NiZn-Gly, and NiZnMnMgSr-Gly particles at 10⁻⁵ dilutions are shown in Figure 4b. *In vitro* CFU test results indicate that upon

incorporating the variety of principal metal cations in the glycerol matrix, bacterial growth was exponentially increased.

To better understand if the glycerol matrix is effective in enhancing bacterial growth, some of the NiZnMnMgSr-Gly particles were annealed to remove glycerol content. Figure S4 shows the bactericidal efficiency of (NiZnMnMgSr)₃O₄ polyelemental metal oxide particles, which were synthesized by annealing quinary NiZnMnMgSr-Gly particles in an air atmosphere at 800 °C for 3 h. Figure S4a shows the STEM-EDS elemental mapping of (NiZnMnMgSr)₃O₄ particles, indicating the possibility of phase segregation occurring during the annealing process. Figure S4b shows the CFU test performance of (NiZnMnMgSr)₃O₄ particles (100 μ g/mL), indicating that upon the decomposition of the glycerol matrix, the particles can kill about 40% of E. coli bacteria within 4 h. The corresponding agar plates (CFU 10⁻⁴ dilution) are shown in Figure S4c. It can be concluded that the presence of glycerol is essential to yield effective bacterial growth from PGPs. In the following section, STEM-EDS analysis provides better understanding on why glycerol is important to promote bacterial growth.

To investigate the underlying microscale reasons for bacterial growth in the glycerol containing particles, the graphene liquid cell (GLC) approach⁴⁵⁻⁴⁷ was used to encapsulate E. coli bacteria and PGPs and the specimens were imaged in STEM. Figure 5 shows the STEM-EDS elemental analysis of the interaction of unary Ni-Gly and binary NiZn-Gly particles with E. coli bacteria in an aqueous environment. Figure 5a shows the STEM-HAADF micrograph of unary Ni-Gly particles in contact with E. coli bacteria and corresponding STEM-EDS mixed elemental mapping confirming the presence of Ni, O, C, N, P, and S elements. Figure 5b shows the STEM-EDS elemental mapping of individual Ni, O, C, N, P, and S elements. Herein, Ni, C, and O correspond to unary Ni-Gly particles, while N, P, and S elements, along with C and O, correspond to diagnostic ions in E. coli bacteria. The detection of these diagnostic ions in E. coli bacteria can provide insights on the cellular structural integrity. 44 Sulfur is an integral building block of the bacterial cell membrane and cytoplasmic proteins, mainly in cysteine and methionine amino acids. 48 Phosphorus is present in deoxyribonucleic acid (DNA), phospholipids, and phosphorylated proteins in the bacterial cell. 48,49 Nitrogen as a major constituent in all amino acids can be predominantly traced in the bacterial cell.⁵⁰ Carbon and oxygen are present in all organic cellular components in the cytoplasm and bacterial cell membrane. 50,51 STEM-EDS elemental mapping of Ni confirmed the presence of nickel element in bacteria upon interacting with unary Ni-Gly particles. Interestingly, the Ni-Gly particles were coated with N, P, and S elements that are representative of bacterial diagnostic elements, suggesting the possible formation of biofilm on the glycerolate particles.

Similar release of metal ions was observed for binary and quinary glycerol-containing particles. Figure 5c shows the STEM-HAADF micrograph of binary NiZn-Gly particles in contact with *E. coli* bacteria and the corresponding STEM-EDS mixed elemental maps confirming the presence of Ni, Zn O, C, N, and S elements. Figure 5d shows the STEM-EDS elemental mapping of individual Ni, Zn, O, and C elements corresponding to glycerolate particles and N and S elements, along with C and O, corresponding to diagnostic elements in *E. coli* bacteria. Similar to the unary Ni-Gly particles, STEM-EDS results confirmed that the binary NiZn-Gly particles also

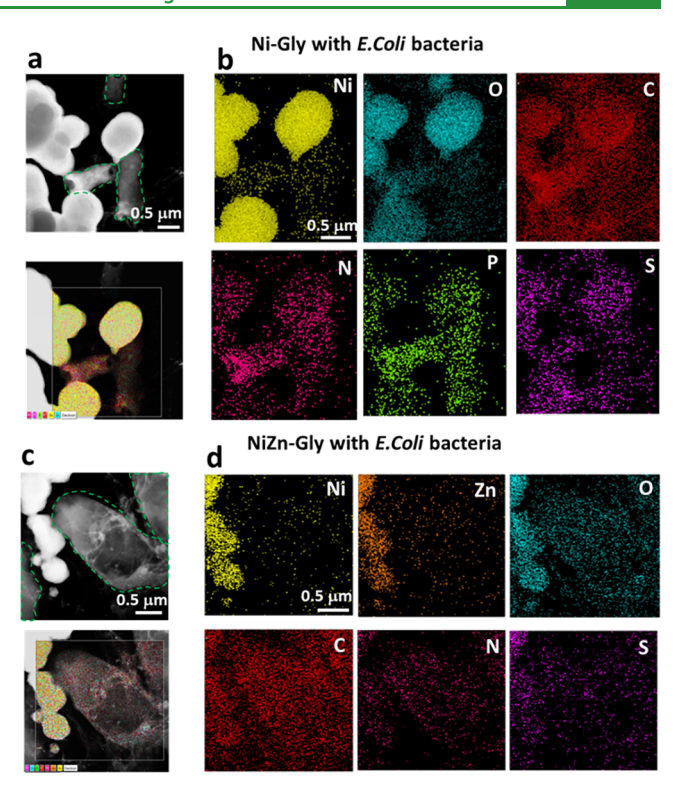


Figure 5. STEM-EDS elemental analysis of *E. coli* bacteria in the presence of unary Ni-Gly and NiZn-Gly particles acquired in a graphene liquid cell aqueous environment. (a) STEM-HAADF micrograph of unary Ni-Gly particles in contact with *E. coli* bacteria and the corresponding STEM-EDS mixed elemental mapping confirming the presence of Ni, O, C, N, P, and S elements. Green dotted lines highlight the bacteria. (b) STEM-EDS elemental mapping of diagnostic Ni, C, O, N, P, and S elements indicating biofilm formation on metal glycerolate particles. (c) STEM-HAADF micrograph of binary NiZn-Gly particles in contact with *E. coli* bacterium and the corresponding STEM-EDS mixed elemental maps confirming the presence of Ni, Zn, O, C, N, and S elements. (d) STEM-EDS elemental maps of diagnostic Ni, Zn C, O, N, and S elements indicating biofilm formation on binary metal glycerolate particles and traces of released metal elements in bacteria.

released Ni and Zn metal elements in the vicinity of the bacteria. Bacterial biofilm diagnostic components, N and S elements, were also detected on binary NiZn-Gly particles. These STEM-EDS results confirmed that the bacterial membrane was not damaged upon interacting with PGPs and cellular integrity was maintained. Figure S5 shows the STEM-EDS elemental analysis of *E. coli* bacteria in the presence of quinary NiZnMnMgSr-Gly particles acquired in a GLC aqueous environment. Results show that Mn and Zn metal elements released from quinary NiZnMnMgSr-Gly particles are detectable in the bacterium cytoplasm.

The effectiveness of glycerol-containing particles for bacterial growth enhancement can also be seen from the formation of biofilms around PGPs. Figure 6a—c provides the evidence of biofilm formation on the surface of quinary metal glycerolate particles upon 2 h of interaction with *E. coli* bacteria. Figure 6a shows the SEM micrograph of quinary NiZnMnMgSr-Gly particles in the absence of bacteria. In Figure 6b,c, a bacterial biofilm thread-like structure 52,53 covering the surface of quinary NiZnMnMgSr-Gly particles upon 2 h of interaction with *E. coli* bacteria can be observed. The SEM results are in agreement with STEM-EDS results

ACS Applied Bio Materials www.acsabm.org Article

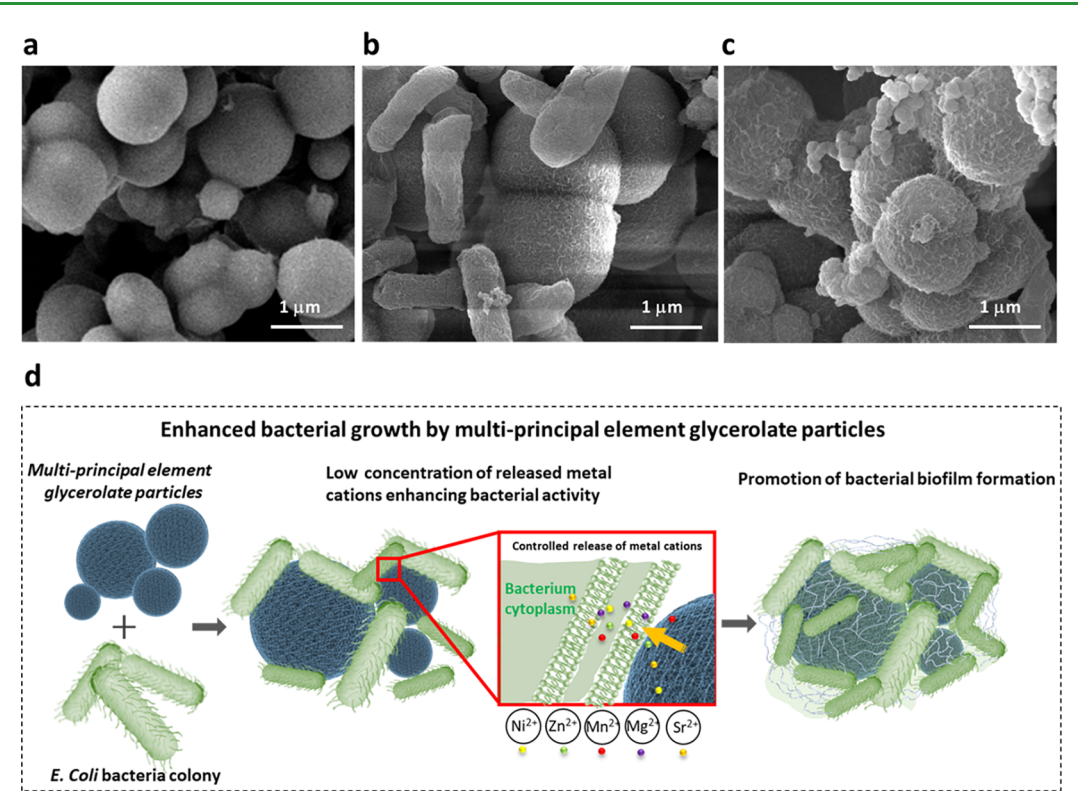


Figure 6. SEM micrographs confirmed the biofilm formation on polyelemental glycerolate particles in the presence of *E. coli* bacteria. (a) SEM micrograph of the as-synthesized quinary NiZnMnMgSr-Gly particles in the absence of bacteria. (b) SEM micrograph of the quinary NiZnMnMgSr-Gly particles covered with bacterial biofilm in the presence of *E. coli* bacteria. (c) SEM micrograph of an additional region where a thread-like synthesized biofilm can be observed on the surface of glycerolate particles. (d) Schematic representation of the possible pathway of enhanced growth of bacteria via biofilm formation on polyelemental glycerolate particles.

(see Figure 5) where the biofilm diagnostic elements N and S were observed on the metal glycerolate particles upon contact with *E. coli* bacteria.

These results shown in Figures 4, 5, and 6a-c underscore the positive role of glycerol in enhancing the bacterial growth of PGPs. Upon utilizing most of the cellular energy to produce proteins, imbalance and drainage of carbon flux in the central metabolism take place due to the production of gene-encoding products.²⁵ Glycerol can replenish depleted carbon levels in bacteria via the gluconeogenesis pathway of dihydroxyacetone phosphate (DHAP) and the glycolysis pathway of DHAP.²⁴ We believe that the enhancement can be due to two important factors: (1) glycerol can provide a carbon resource for the bacteria metabolism and (2) steady decomposition of glycerol by bacteria triggers a controlled release of metal ions that are below the threshold to kill the bacteria. In order to check if metal ion release is triggered by bacteria's consumption of glycerol, control specimens of PGPs were immersed in water and observed in STEM. Interestingly, no release of ions from PGPs was observed in the absence of bacteria (Figure S6).

The observed exponential growth of bacteria upon interacting with quinary NiZnMnMgSr-Gly particles in comparison with unary Ni-Gly particles could be possibly due to the synergistic effect of multiple metal ions improving the bacterial metabolism. Metal ions are essential for metabolic activities in bacteria. Metal ion homeostasis plays a crucial role for importing and mobilizing metal ions in bacteria while optimizing the intracellular metal ion concentration by operating efflux pumps.²⁷ Metalloregulatory proteins in bacteria are metal-sensing transcription factors that can bind

directly with cognate metal cations.⁵⁴ Mn²⁺ and Fe³⁺ ions with their respective protein cofactors contribute to fundamental cellular processes including respiration, intracellular oxidative stress management, and energy production.⁵⁵ Mn²⁺ ions also play vital role in the bacterial cell sporulation process by interacting with cell division proteins.⁵⁶ Zn²⁺ metalloproteins are crucial for structural and enzymatic cofactors in bacteria.⁵⁷ Mg²⁺ ions possess the capability to trigger the production of exopolysaccharides and stabilize the bacterial biofilm.⁵⁸ Exopolysaccharides serve as a scaffold for supporting proteins, carbohydrates, lipids, and nucleic acids.⁵⁹ The hydrogenase process is extremely important for bacterial energy metabolism, which catalyzes the reversible oxidation of hydrogen gas.⁶⁰ Ni²⁺ ions can stimulate the transcription of the hydrogenase genes. 61 Bacterial biofilm consists of DNA, proteins, extracellular polysaccharides, and channels for water and nutrients.⁶² Recently, Shafeeq et al.⁶³ showed that bacterial biofilm formation can be triggered in the presence of Mn²⁺ metal ions. The combination of Mn²⁺ cations and glycerol can stimulate the biofilm formation.⁶⁴ The signal-sensing histidine kinase energy transfer enzymes in bacteria can stimulate sporulation and biofilm formation upon sensing the Mnglycerol matrix.

Figure 6d highlights the schematic representation of the possible pathway for the promotion of bacterial growth in the presence of PGPs. The controlled release of low dosages of metal cations from the glycerol matrix of PGPs is triggered by the presence of bacteria. The synergistic effect of metal cations at such a low dosage is likely to be effective in improving bacterial metabolism. This is evident by the promotion of

biofilm formation over PGPs. We believe that additional studies investigating the controlled release of metal ions from the PGPs in the vicinity of bacterial cells can be insightful. It will be interesting to evaluate the effectiveness of PGPs for the growth of Gram-positive bacteria growth as well.

The present work highlights the enormous potential of PGPs to promote bacterial growth. Bacterial growth kinetics play a crucial role in probiotic bacteria's industrial applications in food nutrition and medicine fields. PGPs can also be utilized for industrial applications in proteomics to reduce the process time in expressing heterologous recombinant proteins by improving the growth kinetics of bacteria. E. coli bacteria require ~20 min of doubling time in glucose salt media under the optimal environmental conditions. The results indicate that quinary NiZnMnMgSr-Gly particles could increase E. coli bacterial growth by 7.3 times in comparison with untreated control E. coli bacteria, confirming a significant reduction in the doubling time of E. coli bacteria.

CONCLUSIONS

In summary, this study confirms enhanced bacterial growth upon interacting with PGPs. The structural and spectroscopy results indicate the layered structure of PGPs and the coordination between the metal cations and glycerol matrix. Chemical mapping at the nanoscale of unary Ni-Gly, binary NiZn-Gly, and quinary NiZnMnMgSr-Gly particles confirmed the homogeneous distribution of metal cations in the glycerol matrix. Colony-counting method results showed 2.7-fold, 3.5fold, and 7.3-fold exponential growth of E. coli bacteria upon 4 h of interaction with unary Ni-Gly, binary NiZn-Gly, and quinary NiZnMnMgSr-Gly particles, respectively, with respect to control E. coli bacteria. GLC-STEM results on aqueous solutions of bacteria and PGPs confirmed the release of metal cations in the bacterium cytoplasm from the glycerol matrix. The membrane of bacteria was intact without causing any cytoplasmic leakage while in contact with unary Ni-Gly, binary NiZn-Gly, and quinary NiZnMnMgSr-Gly particles. Results also indicate that the diagnostic N, P, and S elements of bacteria biofilm were deposited on PGPs. The SEM analysis of PGPs upon 2 h of interaction with cultured E. coli bacteria confirmed bacterial biofilm growth on PGPs. It was determined that the presence of glycerol is effective as a template for the controlled release of metal ions from PGPs. Synergistic release of multiple metal cations from PGPs promoting the biofilm formation was evaluated to be a primary reason for the exponential bacterial growth.

■ METHODS

Synthesis of the Polyelemental Glycerolate Particles. PGPs were synthesized by a facile one-step solvothermal method. 42,67 To synthesize quinary NiZnMnMgSr-Gly particles, equimolar (0.5 mM) concentrations of nickel acetate Ni(CH₃COO)₂·4H₂O, strontium acetate Sr(CH₃COO)₂, manganese acetate Mn(CH₃COO)₂·4H₂O, magnesium acetate Mg(CH₃COO)₂·4H₂O, and zinc acetate Zn-(CH₃COO)₂·2H₂O were dissolved in 40 mL of isopropyl alcohol under continuous stirring for 10 min. Successively, 8 mL of glycerol was added to the mixture, and the solution was stirred for 2 h. The reaction solution was then transferred to a Teflon-lined stainless-steel autoclave container and was kept at 180 °C for 10 h. The final product was separated by centrifugation, rinsed with ethanol, and dried at 60 °C for 24 h. For unary Ni-Gly and binary NiZn-Gly particles, respective metal salt precursors were used following the same synthesis protocol. The obtained yields of synthesized PGPs from 2.5 mM of metallic precursors were 311, 334, and 301 mg for

Ni-Gly, NiZn-Gly, and NiZnMnMgSr-Gly particles, respectively. As an observation, we would like to mention that under the same synthesis conditions, in the absence of metal salt precursors, only glycerolate particles with the same morphology could not be produced.

Characterization of Polyelemental Glycerolate Particles. The XRD crystal structure analysis of unary Ni-Gly particles was performed by using a Bruker nano-Discover 8 instrument. The XRD scan was acquired in the 5 and 90° range of 2θ diffraction angles using 1600 W power at 0.05 2θ resolution with a 1.5 s time step. The FTIR spectrum of unary Ni-Gly particles was obtained using a Bruker ALPHA FTIR spectrometer with an attenuated total reflectance (ATR) accessory. The spectrum was obtained using a 2 cm⁻¹ wavenumber resolution and a working window between 4000 and 400 cm⁻¹. A total of 32 scans were utilized during the acquisition. SEM morphological characterization of as-synthesized PGPs was performed using JEOL JSM-IT500HR field emission SEM. The synthesized PGPs with platinum coating were analyzed at a 10 keV accelerating voltage and a 8 mm working distance. STEM-EDS elemental analysis of PGPs was performed using an aberrationcorrected JEOL ARM200CF TEM (200 keV) in the STEM mode. STEM-EDS mapping was acquired using the Oxford EDS detector equipped with the drift corrector. The STEM-HAADF images were acquired at a 22 mrad convergence angle with 512×512 resolution.

In Vitro Colony Counting Method. The colony counting method is utilized to quantitatively evaluate the interaction of PGPs with gram-negative *E. coli* bacteria (ATCC29425). LB agar plates were prepared using the standard manufacturer's instructions. The bacteria were cultured by inoculating *E. coli* stock in sterilized LB broth medium and by incubating for 16 h at 37 °C under shaking to achieve 10⁸ CFU/mL concentration. Successively, cultured *E. coli* bacteria were treated with a 100 μg/mL concentration of unary Ni-Gly, binary NiZn-Gly, and quinary NiZnMnMgSr-Gly particles for 6 h. Upon interaction, the culture was diluted to 10⁻⁵ using serial dilutions. Twenty microliters of each dilution were spread onto LB agar plates. The agar plates were incubated overnight to evaluate the colony-forming units. The experiments were performed in the duplicates for each dilution. Bactericidal growth was calculated with respect to the control bacteria (without treating with PGPs) sample.

In Situ Graphene Liquid Cell–STEM Analysis of Bacteria and Polyelemental Glycerol Particles. Graphene-coated TEM grids were prepared by using a protocol described by Hauwiller et al. 68 Briefly, monolayer commercially CVD grown graphene-coated copper foil was cut into a 1 cm \times 1 cm piece using a surgical-grade scalpel. The quantifoil micromachined holey carbon coated 200 mesh gold grids (SPI supplies, 4220G-XA) were placed on the graphene-coated copper foil by ensuring that the carbon layer of the grids remains in contact with graphene. Successively, 15 μ L of isopropyl alcohol was dropped on the graphene-coated copper foil to obtain better contact between the grids and the copper foil After 2 h of drying, graphene-coated copper foil along with TEM grids were placed in the sodium persulfate solution copper etchant for 12 h. After copper foil etching, floating gold TEM grids were rinsed using deionized water and allowed to air-dry at room temperature.

To perform in situ GLC-STEM studies of PGPs interaction with bacteria, first, the cultured $E.\ coli$ bacteria were rinsed with DI water. The bacteria suspension with a concentration of 100 CFU/mL was mixed with PGPs at 25 μ g/mL and allowed to interact for 30 min. The reaction solution droplet was encapsulated between two graphene-coated TEM grids to fabricate the graphene liquid cells. The STEM-EDS analysis of encapsulated bacteria with PGPs was performed using a JEOL ARM200CF aberration-corrected 200 keV microscope. The emission current of the electron beam was reduced up to $10\ \mu$ A during EDS acquisition. The maximum electron dose rate of $0.34\ e^-/Å^2/s$ was maintained to avoid electron beam damage.

SEM Characterization of Bacterial Biofilm Formation. To evaluate the bacterial biofilm formation, SEM characterization was utilized. To prepare the bacterial biofilm samples for SEM analysis, the cultured *E. coli* bacteria suspended in deionized water were dropped on quinary NiZnMnMgSr-Gly particles placed on the glass

slide. The glass slide with bacteria and the quinary NiZnMnMgSr-Gly particles was incubated at 37 $^{\circ}$ C for 2 h. For fixation, the specimen glass slide was immersed in 2.5% glutaraldehyde for 2 h at 4 $^{\circ}$ C temperature. Successively, the specimen glass slide was rinsed for 5 min using 30, 50, 70, 80, 95, and 100% ethanol baths. Finally, the glass slide was dehydrated using 50 and 100% hexamethyldisilazane (HMDS) solution, and the sample was coated with a 10 nm platinum layer for SEM analysis. SEM characterization was performed using a JEOL JSM-IT500HR field emission SEM operating at a 10 keV accelerating voltage.

ASSOCIATED CONTENT

Solution Supporting Information

The Supporting Information is available free of charge at https://pubs.acs.org/doi/10.1021/acsabm.2c01052.

(Figure S1) XRD spectrum of NiZnMnMgSr-Gly particles; (Figure S2) XRD spectrum of NiZn-Gly particles; (Figure S3) STEM-HAADF micrographs of unary Ni-Gly, binary NiZn-Gly, and quinary NiZnMnMgSr-Gly particles from which the STEM-EDS elemental mapping was acquired; (Figure S4) in vitro antibacterial activity of (Ni, Zn, Mn, Mg, or Sr)₃O₄ polyelemental metal oxide particles (PMOPs) synthesized by annealing quinary NiZnMnMgSr-Gly particles in air atmosphere at 800 °C for 3 h; (Figure S5) STEM-EDS elemental analysis of *E. coli* bacteria in the presence of quinary NiZnMnMgSr-Gly particles acquired in graphene liquid cell aqueous environment; (Figure S6) STEM-EDS analysis of unary Ni-Gly particles acquired in GLC aqueous environment; (Table S1) highlighting the summary of maximum tolerance limit of metal cations beneficial for bacterium metabolism (PDF)

■ AUTHOR INFORMATION

Corresponding Authors

Tolou Shokuhfar — Department of Biomedical Engineering, University of Illinois at Chicago, Chicago, Illinois 60607, United States; Email: tolou@uic.edu

Reza Shahbazian-Yassar — Department of Mechanical & Industrial Engineering, University of Illinois at Chicago, Chicago, Illinois 60607, United States; oocid.org/0000-0002-7744-4780; Email: rsyassar@uic.edu

Authors

Abhijit H. Phakatkar — Department of Biomedical Engineering, University of Illinois at Chicago, Chicago, Illinois 60607, United States

Josué M. Gonçalves — Department of Mechanical & Industrial Engineering, University of Illinois at Chicago, Chicago, Illinois 60607, United States; Department of Fundamental Chemistry, University of Sao Paulo, Sao Paulo, SP 05508-060, Brazil; orcid.org/0000-0003-0800-077X

Jianshu Zhou – Department of Biomedical Engineering, University of Illinois at Chicago, Chicago, Illinois 60607, United States

Timothy G. Ritter — Department of Civil, Materials, and Environmental Engineering, University of Illinois at Chicago, Chicago, Illinois 60607, United States; occid.org/0000-0002-5139-1908

Mahmoud Tamadoni Saray — Department of Mechanical & Industrial Engineering, University of Illinois at Chicago, Chicago, Illinois 60607, United States

Lioudmila V. Sorokina — Department of Civil, Materials, and Environmental Engineering, University of Illinois at Chicago, Chicago, Illinois 60607, United States

Azadeh Amiri — Department of Mechanical & Industrial Engineering, University of Illinois at Chicago, Chicago, Illinois 60607, United States

Lucio Angnes – Department of Fundamental Chemistry, University of Sao Paulo, Sao Paulo, SP 05508-060, Brazil

Complete contact information is available at: https://pubs.acs.org/10.1021/acsabm.2c01052

Author Contributions

A.H.P. performed the in situ GLC STEM and in vitro bacteria—PGP interaction experiments and wrote the manuscript. J.M.G. and L.A. synthesized the PGPs and performed FTIR characterization. J.Z. contributed in bacteria culture and in vitro bacteria experiments. T.G.R. performed XRD characterization of the experiments. L.V.S. and A.A. contributed to investigating bacteria growth mechanisms upon treating with PGPs. R.S.Y. and T.S. conceptualized and supervised the project. All authors proofread, commented on, and approved the final manuscript for submission.

Notes

The authors declare no competing financial interest.

ACKNOWLEDGMENTS

The present work made use of instruments in the Electron Microscopy Core of Research Resources Centre at University of Illinois at Chicago. R.S.-Y. is thankful to the National Science Foundation (NSF) for award number DMR1809439. T.S. acknowledges financial support from NSF award number DMR-1710049. Partial support from NSF award number CDS&E-2055442 is also acknowledged. The authors acknowledge financial support from FAPESP for their support (projects 2017/13137-5). In addition, we thank the fellowship granted to J.M.G. (FAPESP 2018/16896-7 and 2020/06176-7). We thank Prof. Koiti Araki and Irlan S. Lima (Laboratório de Química Supramolecular e Nanotecnologia, IQ-USP) and SisNANO USP for the use of the FTIR spectroscopy facility.

ABBREVIATIONS

E. coli Escherichia coli

PGPs polyelemental glycerolate particles

GLC graphene liquid cell

STEM scanning transmission electron microscopy

TEM transmission electron microscopy EDS energy-dispersive X-ray spectroscopy

HAADF high-angle annular dark field

CFU colony-forming units XRD X-ray diffraction

FTIR Fourier transform infrared spectroscopy

DHAP dihydroxyacetone phosphate ATR attenuated total reflectance HMDS hexamethyldisilazane

PMOPs polyelemental metal oxide particles

REFERENCES

(1) Chen, P.-C.; Liu, M.; Du, J. S.; Meckes, B.; Wang, S.; Lin, H.; Dravid, V. P.; Wolverton, C.; Mirkin, C. A. Interface and heterostructure design in polyelemental nanoparticles. *Science* **2019**, *363*, 959–964.

- (2) Chen, P.-C.; Liu, X.; Hedrick, J. L.; Xie, Z.; Wang, S.; Lin, Q.-Y.; Hersam, M. C.; Dravid, V. P.; Mirkin, C. A. Polyelemental nanoparticle libraries. *Science* **2016**, *352*, 1565–1569.
- (3) Yao, Y.; Huang, Z.; Xie, P.; Lacey, S. D.; Jacob, R. J.; Xie, H.; Chen, F.; Nie, A.; Pu, T.; Rehwoldt, M.; Yu, D.; Zachariah, M. R.; Wang, C.; Shahbazian-Yassar, R.; Li, J.; Hu, L. Carbothermal shock synthesis of high-entropy-alloy nanoparticles. *Science* **2018**, 359, 1489–1494.
- (4) Abdullah, M. I.; Hameed, A.; Zhang, N.; Ma, M. Ultrasonic-Assisted Synthesis of Amorphous Polyelemental Hollow Nanoparticles as Efficient and Stable Bifunctional Electrocatalysts for Overall Water Splitting. *Adv. Mater. Interfaces* **2019**, *6*, 1900586.
- (5) Wu, M.; Cui, M.; Wu, L.; Hwang, S.; Yang, C.; Xia, Q.; Zhong, G.; Qiao, H.; Gan, W.; Wang, X.; Kline, D.; Zachariah, M. R.; Su, D.; Li, T.; Hu, L. Hierarchical polyelemental nanoparticles as bifunctional catalysts for oxygen evolution and reduction reactions. *Adv. Energy Mater.* **2020**, *10*, 2001119.
- (6) Petrini, L.; Migliavacca, F. Biomedical applications of shape memory alloys. *J. Metall.* **2011**, 2011, 501483.
- (7) Ramalingam, V. V.; Ramasamy, P.; Kovukkal, M. D.; Myilsamy, G. Research and development in magnesium alloys for industrial and biomedical applications: a review. *Met. Mater. Int.* **2020**, *26*, 409–430.
- (8) Koo, W.-T.; Millstone, J. E.; Weiss, P. S.; Kim, I.-D. The design and science of polyelemental nanoparticles. *ACS Nano* **2020**, *14*, 6407–6413.
- (9) Alamdari, A. A.; Hashemkhani, M.; Hendessi, S.; Guner, P. T.; Acar, H. Y.; Kavakli, I. H.; Unal, U.; Motallebzadeh, A. In vitro antibacterial and cytotoxicity assessment of magnetron sputtered Ti1. SZrTa0. 5Nb0. 5W0. 5 refractory high-entropy alloy doped with Ag nanoparticles. *Vacuum* **2022**, 203, No. 111286.
- (10) Murray, A. F.; Bryan, D.; Garfinkel, D. A.; Jogensen, C. S.; Tang, N.; Liyanage, W.; Lass, E. A.; Yang, Y.; Rack, P. D.; Denes, T. G. Anti-microbial properties of a multi-component alloy. *Sci. Rep.* **2022**, *12*, 21427.
- (11) Wang, J.; Lin, H.; Chuang, W.; Chuang, C.; Lin, Y.-H.; Huang, J.; Lin, Y.-H. Laser dewetting mechanism and antibacterial properties of Cu-Al based medium entropy alloy films. *J. Alloys Compd.* **2022**, 903, No. 163893.
- (12) Ozan, S.; Lin, J.; Li, Y.; Wen, C. New Ti-Ta-Zr-Nb alloys with ultrahigh strength for potential orthopedic implant applications. *J. Mech. Behav. Biomed. Mater.* **2017**, *75*, 119–127.
- (13) Prodana, M.; Nistor, C.-E.; Stoian, A. B.; Ionita, D.; Burnei, C. Dual nanofibrous bioactive coatings on TiZr implants. *Coatings* **2020**, *10*, 526.
- (14) Amiri, A.; Shahbazian-Yassar, R. Recent progress of high-entropy materials for energy storage and conversion. *J. Mater. Chem. A* **2021**, *9*, 782–823.
- (15) Chen, C.; Chen, J.; Yuan, S.; Li, W.; Wang, W.; Li, X.; Zhang, W.; Wei, R.; Guan, S.; Wang, T.; Zhang, T.; Lei, N.; Li, F. Microstructure, mechanical properties, corrosion resistance and anti-bacterial behavior of novel Co-free high entropy alloys. *J. Alloys Compd.* 2022, 902, No. 163714.
- (16) Apollon, W.; Luna-Maldonado, A. I.; Kamaraj, S.-K.; Vidales-Contreras, J. A.; Rodríguez-Fuentes, H.; Gómez-Leyva, J. F.; Aranda-Ruíz, J. Progress and recent trends in photosynthetic assisted microbial fuel cells: a review. *Biomass Bioenergy* **2021**, *148*, No. 106028.
- (17) Cid, F. P.; Rilling, J. I.; Graether, S. P.; Bravo, L. A.; Mora, M. D. L. L.; Jorquera, M. A. Properties and biotechnological applications of ice-binding proteins in bacteria. *FEMS Microbiol. Lett.* **2016**, *363*, fnw099.
- (18) Bhuyan, D. J.; Basu, A., Phenolic compounds potential health benefits and toxicity. In *Utilisation of bioactive compounds from agricultural and food waste*, CRC Press: 2017; pp. 27–59.
- (19) Darwish, M. S.; Qiu, L.; Taher, M. A.; Zaki, A. A.; Abou-Zeid, N. A.; Dawood, D. H.; Shalabi, O. M.; Khojah, E.; Elawady, A. A. Health Benefits of Postbiotics Produced by E. coli Nissle 1917 in Functional Yogurt Enriched with Cape Gooseberry (Physalis peruviana L.). Fermentation 2022, 8, 128.

- (20) Klaenhammer, T. R. Probiotic bacteria: today and tomorrow. *J. Nutr.* **2000**, *130*, 415S–416S.
- (21) Secher, T.; Kassem, S.; Benamar, M.; Bernard, I.; Boury, M.; Barreau, F.; Oswald, E.; Saoudi, A. Oral administration of the probiotic strain Escherichia coli Nissle 1917 reduces susceptibility to neuroinflammation and repairs experimental autoimmune encephalomyelitis-induced intestinal barrier dysfunction. *Front. Immunol.* **2017**, *8*, 1096.
- (22) Wang, Y.; Wu, Y.; Wang, Y.; Xu, H.; Mei, X.; Yu, D.; Wang, Y.; Li, W. Antioxidant properties of probiotic bacteria. *Nutrients* **2017**, *9*, 521
- (23) Lee, P. S.; Lee, K. H. Escherichia coli—a model system that benefits from and contributes to the evolution of proteomics. *Biotechnol. Bioeng.* **2003**, *84*, 801–814.
- (24) Chiang, C.-J.; Ho, Y.-J.; Hu, M.-C.; Chao, Y.-P. Rewiring of glycerol metabolism in Escherichia coli for effective production of recombinant proteins. *Biotechnol. Biofuels* **2020**, *13*, 1–9.
- (25) Gill, R.; Valdes, J.; Bentley, W. A comparative study of global stress gene regulation in response to overexpression of recombinant proteins in Escherichia coli. *Metab. Eng.* **2000**, *2*, 178–189.
- (26) Murarka, A.; Dharmadi, Y.; Yazdani, S. S.; Gonzalez, R. Fermentative utilization of glycerol by Escherichia coli and its implications for the production of fuels and chemicals. *Appl. Environ. Microbiol.* **2008**, *74*, 1124–1135.
- (27) Chandrangsu, P.; Rensing, C.; Helmann, J. D. Metal homeostasis and resistance in bacteria. *Nat. Rev. Microbiol.* **2017**, 15, 338–350.
- (28) Begg, S. L. The role of metal ions in the virulence and viability of bacterial pathogens. *Biochem. Soc. Trans.* **2019**, *47*, 77–87.
- (29) Waldron, K. J.; Robinson, N. J. How do bacterial cells ensure that metalloproteins get the correct metal? *Nat. Rev. Microbiol.* **2009**, 7, 25–35.
- (30) Mir, N.; Salavati-Niasari, M.; Davar, F. Preparation of ZnO nanoflowers and Zn glycerolate nanoplates using inorganic precursors via a convenient rout and application in dye sensitized solar cells. *Chem. Eng. J.* **2012**, *181*, 779–789.
- (31) Chivers, P. T.; Sauer, R. T. Regulation of high affinity nickel uptake in bacteria: Ni2+—dependent interaction of NikR with wild-type and mutant operator sites. *J. Biol. Chem.* **2000**, 275, 19735—19741.
- (32) Outten, C. E.; O'Halloran, A. V. T. Femtomolar sensitivity of metalloregulatory proteins controlling zinc homeostasis. *Science* **2001**, 292, 2488–2492.
- (33) Ma, Z.; Jacobsen, F. E.; Giedroc, D. P. Coordination chemistry of bacterial metal transport and sensing. *Chem. Rev.* **2009**, *109*, 4644–4691
- (34) Wu, R. X.; Zhang, Y.; Guo, Z. Q.; Zhao, B.; Guo, J. S. Role of Ca2+ and Mg2+ in changing biofilm structure and enhancing biofilm formation of P. stutzeri strain XL-2. *Colloids Surf.*, B **2022**, No. 112972.
- (35) Achal, V.; Pan, X.; Zhang, D. Bioremediation of strontium (Sr) contaminated aquifer quartz sand based on carbonate precipitation induced by Sr resistant Halomonas sp. *Chemosphere* **2012**, *89*, 764–768.
- (36) Anbu, P.; Kang, C.-H.; Shin, Y.-J.; So, J.-S. Formations of calcium carbonate minerals by bacteria and its multiple applications. *Springerplus* **2016**, *5*, 1–26.
- (37) Lau, P.-C.; Kwong, T.-L.; Yung, K.-F. Effective heterogeneous transition metal glycerolates catalysts for one-step biodiesel production from low grade non-refined Jatropha oil and crude aqueous bioethanol. *Sci. Rep.* **2016**, *6*, 1–10.
- (38) Li, K.; Zhang, R.; Gao, R.; Shen, G.-Q.; Pan, L.; Yao, Y.; Yu, K.; Zhang, X.; Zou, J.-J. Metal-defected spinel MnxCo3-xO4 with octahedral Mn-enriched surface for highly efficient oxygen reduction reaction. *Appl. Catal., B* **2019**, 244, 536–545.
- (39) Zhang, R.; Zhang, Y.-C.; Pan, L.; Shen, G.-Q.; Mahmood, N.; Ma, Y.-H.; Shi, Y.; Jia, W.; Wang, L.; Zhang, X.; Xu, W.; Zou, J. J. Engineering cobalt defects in cobalt oxide for highly efficient electrocatalytic oxygen evolution. ACS Catal. 2018, 8, 3803–3811.

- (40) Hong, J.; Heo, S. J.; Singh, P. Water mediated growth of oriented single crystalline SrCO3 nanorod arrays on strontium compounds. *Sci. Rep.* **2021**, *11*, 1–11.
- (41) Alhawi, T.; Rehan, M.; York, D.; Lai, X. Hydrothermal synthesis of zinc carbonate hydroxide nanoparticles. *Procedia Eng.* **2015**, *102*, 356–361.
- (42) Wang, M.; Jiang, J.; Ai, L. Layered bimetallic iron—nickel alkoxide microspheres as high-performance electrocatalysts for oxygen evolution reaction in alkaline media. *ACS Sustainable Chem. Eng.* **2018**, *6*, 6117—6125.
- (43) Angelidou, A.; Conti, M.-G.; Diray-Arce, J.; Benn, C. S.; Shann, F.; Netea, M. G.; Liu, M.; Potluri, L. P.; Sanchez-Schmitz, G.; Husson, R.; Ozonoff, A.; Kampmann, B.; van Haren, S. D.; Levy, O. Licensed Bacille Calmette-Guérin (BCG) formulations differ markedly in bacterial viability, RNA content and innate immune activation. *Vaccine* 2020, 38, 2229–2240.
- (44) Phakatkar, A. H.; Firlar, E.; Alzate, L.; Song, B.; Narayanan, S.; Rojaee, R.; Foroozan, T.; Deivanayagam, R.; Banner, D. J.; Shahbazian-Yassar, R.; Shokuhfar, T. TEM studies on antibacterial mechanisms of black phosphorous nanosheets. *Int. J. Nanomed.* **2020**, *15*, 3071.
- (45) Firlar, E.; Ouy, M.; Bogdanowicz, A.; Covnot, L.; Song, B.; Nadkarni, Y.; Shahbazian-Yassar, R.; Shokuhfar, T. Investigation of the magnetosome biomineralization in magnetotactic bacteria using graphene liquid cell–transmission electron microscopy. *Nanoscale* **2019**, *11*, 698–705.
- (46) He, K.; Shokuhfar, T.; Shahbazian-Yassar, R. Imaging of soft materials using in situ liquid-cell transmission electron microscopy. *J. Phys.: Condens. Matter* **2019**, *31*, 103001.
- (47) Yuk, J. M.; Park, J.; Ercius, P.; Kim, K.; Hellebusch, D. J.; Crommie, M. F.; Lee, J. Y.; Zettl, A.; Alivisatos, A. P. High-resolution EM of colloidal nanocrystal growth using graphene liquid cells. *Science* **2012**, 336, 61–64.
- (48) Liu, J. L.; Luo, Z.; Bashir, S. A progressive approach on inactivation of bacteria using silver—titania nanoparticles. *Biomater. Sci.* **2013**, *1*, 194—201.
- (49) Feng, Q. L.; Wu, J.; Chen, G. Q.; Cui, F.; Kim, T.; Kim, J. A mechanistic study of the antibacterial effect of silver ions on Escherichia coli and Staphylococcus aureus. *J. Biomed. Mater. Res.* **2000**, *52*, 662–668.
- (50) Mesibov, R.; Adler, J. Chemotaxis toward amino acids in Escherichia coli. *J. Bacteriol.* **1972**, *112*, 315–326.
- (51) Fagerbakke, K. M.; Heldal, M.; Norland, S. Content of carbon, nitrogen, oxygen, sulfur and phosphorus in native aquatic and cultured bacteria. *Aquat. Microb. Ecol.* **1996**, *10*, 15–27.
- (52) Bridier, A.; Sanchez-Vizuete, M. D. P.; Le Coq, D.; Aymerich, S.; Meylheuc, T.; Maillard, J.-Y.; Thomas, V.; Dubois-Brissonnet, F.; Briandet, R. Biofilms of a Bacillus subtilis hospital isolate protect Staphylococcus aureus from biocide action. *PLoS One* **2012**, *7*, No. e44506.
- (53) Hoque, E.; Fritscher, J. Ecology, adaptation, and function of methane-sulfidic spring water biofilm microorganisms, including a strain of anaerobic fungus Mucor hiemalis. *MicrobiologyOpen* **2017**, *6*, No. e00483.
- (54) Waldron, K. J.; Rutherford, J. C.; Ford, D.; Robinson, N. J. Metalloproteins and metal sensing. *Nature* **2009**, *460*, 823–830.
- (55) Jakubovics, N. S.; Jenkinson, H. F. Out of the iron age: new insights into the critical role of manganese homeostasis in bacteria. *Microbiology* **2001**, *147*, 1709–1718.
- (56) Mhatre, E.; Troszok, A.; Gallegos-Monterrosa, R.; Lindstädt, S.; Hölscher, T.; Kuipers, O. P.; Kovács, Á. T. The impact of manganese on biofilm development of Bacillus subtilis. *Microbiology* **2016**, *162*, 1468–1478.
- (57) Andreini, C.; Banci, L.; Bertini, I.; Rosato, A. Zinc through the three domains of life. *J. Proteome Res.* **2006**, *5*, 3173–3178.
- (58) Song, B.; Leff, L. G. Influence of magnesium ions on biofilm formation by Pseudomonas fluorescens. *Microbiol. Res.* **2006**, *161*, 355–361.

- (59) Rabin, N.; Zheng, Y.; Opoku-Temeng, C.; Du, Y.; Bonsu, E.; Sintim, H. O. Biofilm formation mechanisms and targets for developing antibiofilm agents. *Future Med. Chem.* **2015**, *7*, 493–512.
- (60) Mulrooney, S. B.; Hausinger, R. P. Nickel uptake and utilization by microorganisms. *FEMS Microbiol. Rev.* **2003**, *27*, 239–261.
- (61) Kim, H.; Yu, C.; Maier, R. Common cis-acting region responsible for transcriptional regulation of Bradyrhizobium japonicum hydrogenase by nickel, oxygen, and hydrogen. *J. Bacteriol.* **1991**, 173, 3993–3999.
- (62) Flemming, H.-C.; Neu, T. R.; Wozniak, D. J. The EPS matrix: the "house of biofilm cells". *J. Bacteriol.* **2007**, *189*, 7945–7947.
- (63) Shafeeq, S.; Pannanusorn, S.; Elsharabasy, Y.; Ramírez-Zavala, B.; Morschhäuser, J.; Römling, U. Impact of manganese on biofilm formation and cell morphology of Candida parapsilosis clinical isolates with different biofilm forming abilities. *FEMS Yeast Res.* **2019**, 19, foz057.
- (64) Shemesh, M.; Chai, Y. A combination of glycerol and manganese promotes biofilm formation in Bacillus subtilis via histidine kinase KinD signaling. *J. Bacteriol.* **2013**, *195*, 2747–2754.
- (65) Rosano, G. L.; Ceccarelli, E. A. Recombinant protein expression in Escherichia coli: advances and challenges. *Front. Microbiol.* **2014**, *5*, 172
- (66) Newman, E.; Budman, L.; Chan, E.; Greene, R.; Lin, R.; Woldringh, C.; D'Ari, R. Lack of S-adenosylmethionine results in a cell division defect in Escherichia coli. *J. Bacteriol.* **1998**, *180*, 3614—3619
- (67) Zhu, L.; Lu, H.; Xiao, F.; Yao, T.; Liu, T.; Li, F.; Wang, J.; Han, X.; Cheng, Y.; Wang, H. Flower-like Mn/Co Glycerolate-Derived α -MnS/Co9S8/Carbon Heterostructures for High-Performance Lithium-Ion Batteries. *ACS Appl. Energy Mater.* **2020**, *3*, 10215–10223.
- (68) Hauwiller, M. R.; Ondry, J. C.; Alivisatos, A. P. Using graphene liquid cell transmission electron microscopy to study in situ nanocrystal etching. *J. Visualized Exp.* **2018**, No. e57665.

☐ Recommended by ACS

Defining the Surface Oxygen Threshold That Switches the Interaction Mode of Graphene Oxide with Bacteria

Zhiling Guo, Iseult Lynch, et al.

FEBRUARY 26, 2023

ACS NANO

READ 🗹

In Situ Microscopic Studies on the Interaction of Multi-Principal Element Nanoparticles and Bacteria

Abhijit H. Phakatkar, Reza Shahbazian-Yassar, et al.

MARCH 15, 2023

ACS NANO

READ 🗹

Ionic Strength-Dependent Attachment of *Pseudomonas* aeruginosa PAO1 on Graphene Oxide Surfaces

Xinxin Jing, Noha Mohamed Ashry, et al.

NOVEMBER 15, 2022

ENVIRONMENTAL SCIENCE & TECHNOLOGY

READ 🗹

Nano- and Microplastics Aided by Extracellular Polymeric Substances Facilitate the Conjugative Transfer of Antibiotic Resistance Genes in Bacteria

Xiaomei Liu, John P. Giesy, et al.

NOVEMBER 28, 2022

ACS ES&T WATER

READ 🗹

Get More Suggestions >